CFD PREDICTION OF UNSTEADY PRESSURES DUE TO FAN ROTOR-STATOR INTERACTION

H. Kodama, A. Yamagata and N. Tsuchiya
Ishikawajima-Harima Heavy Industries Co., Ltd.

O. Nozaki, T. Nishizawa and K. Yamamoto
Japan Aerospace Exploration Agency

Keywords: *Aeroengine, Fan Noise, Rotor-Stator Interaction, Unsteady Flow, CFD*

Abstract

Unsteady three-dimensional Navier-Stokes analyses are performed to predict the unsteady pressures induced by rotor viscous wakes on stator vanes. The primary object of this study is to investigate the effects of axial spacing between the rotor and the stator and three-dimensional vane geometries such as stator sweep and stator lean on the unsteady pressure fluctuations on the stator vane.

Five different stator configurations with three sets of stator geometries, which are three radial stator configurations with different axial spacing, the swept stator and the swept and leaned stator, are used for this study.

A three-dimensional analytical method using unsteady lifting-surface theory is also used to elucidate the mechanism of interaction of passing rotor wakes with downstream stator.

It is found that, in axial spacing between rotor and stator, the effect of radial phase skew of incoming rotor wake is important for the reduction in the induced unsteady pressure. It is also shown that incorporation of stator sweep and lean is effective to obtain a significant reduction in the induced unsteady pressure.

Nomenclature

L axial distance between rotor and stator
R radius
V absolute velocity at rotor exit
V_t swirl component of V
V_x axial component of V
q change in the circumferential phase angle of rotor wake during the wake convection from rotor trailing edge to stator leading edge
dq difference in the circumferential phase angle of rotor wake between hub and tip at stator inlet
Ω angular velocity of rotor rotation

1 Introduction

A major source of current high bypass ratio turbofan engine noise comes from fan rotor-stator interaction. The pressure fluctuations induced on the stator vanes as a result of interaction of the rotor viscous wakes with downstream stators generate discrete frequency interaction tones and broadband noise.

Widely used approaches to reduce the fan rotor-stator interaction noise for modern turbofan engines have been to select blade/vane ratios to satisfy the cutoff criterion for propagation of the fundamental rotor tone and increased axial distance between the rotor and the stator. Recently, new attempts to reduce this interaction noise using three dimensional blade geometries, such as swept and/or leaned stator vanes, have been conducted experimentally. A model high-speed fan stage was tested by Woodward et al. [1] to evaluate acoustic benefits associated with a swept and leaned stator and with a swept integral vane/frame stator. Envia [2] measured time histories of vane fluctuating pressures for both a radial and a swept vane configuration. Significant reductions

in sound pressure level were observed for the swept vane relative to the radial vane for blade passing frequency harmonics of vane pressure, but vane broadband noise reductions due to sweep turned out to be much smaller.

A number of analytical studies for a two-dimensional cascade have appeared so far to investigate the unsteady blade forces produced by rotor-stator interaction, however very few efforts exist for a three-dimensional cascade. Namba [3] developed an unsteady lifting-surface theory for a rotating subsonic annular cascade to investigate the three-dimensional effects on the unsteady blade forces and the acoustic power generation caused by interaction of blades with inlet wakes. It was suggested that increasing a radial phase skewing of inlet wakes effectively reduced the generated sound power especially when the number of the super-resonant acoustic modes (cut-on modes) is small. Kodama and Namba [4] extended the analytical method using the unsteady lifting-surface theory to investigate the effects of blade sweep on the acoustic power generated by interaction with a convected sinusoidal gust. It was found that increasing the sweep resulted in remarkable reduction in the acoustic power for both forward and backward sweeps.

A numerical approach to predict the rotor-stator interaction in a high-speed fan stage was acoustically attempted by Tsuchiya et al. [5]. The rotor-stator stage analysis using the three-dimensional unsteady Reynolds-averaged Navier-Stokes equations was conducted for the fan stage with a radial stator to acquire the unsteady pressures induced by the rotor viscous wakes on the stator vanes, and the acoustic field generated by the unsteady pressures in the duct was obtained through an analytical model using the unsteady lifting-surface theory developed by Namba [3], in which the unsteady pressures from the numerical results were imposed on the lifting-surface in the form of pressure differences across the stator vane. The numerical approach was compared with the analytical approach, in which the unsteady pressures induced by the rotor viscous wakes on the stator vanes were also predicted by the unsteady lifting surface theory, and it was shown that the surface distribution of vane unsteady loadings predicted by the numerical method was very similar to that predicted by the analytical method, but the acoustic power level obtained from the numerical results was more realistic than the analytical prediction.

In the present study, the numerical method developed by Tsuchiya et al. [5] was applied to the analyses of five fan configurations with three sets of stator geometries to investigate the effects of axial spacing between the rotor and the stator, stator sweep and stator lean on the unsteady pressures induced by the rotor viscous wakes on the stator vanes.

2 Numerical Procedure

2.1 Computational Scheme

The governing equations are the time-dependent three-dimensional Reynolds-averaged Navier-Stokes equations, and the turbulent viscosity is determined by the two-layer Baldwin-Lomax algebraic turbulence model. An implicit finite difference scheme, which is capable of using a large CFL number, is used for time integration. The convection terms are discretized using the TVD scheme developed by Chakravarthy and Osher and central differencing is used for the

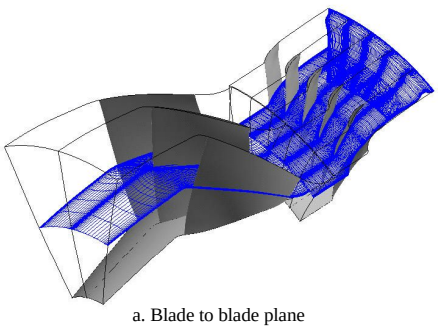

a. Blade to blade plane

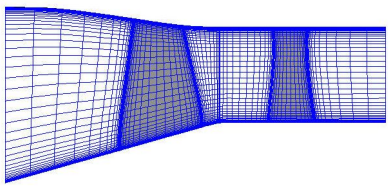

b. Meridional plane

Figure 1. Computational grid for unsteady stage analysis.

diffusion terms. For the implicit time integration approach, a Newton sub-iteration is performed at each time step to increase stability and reduce linearization errors.

A computational domain is divided into sub-domains. The algorithm in the present code is paralleled so that each sub-domain is executed on a different processing element of scalar-paralleled super computer system called Numerical Simulator III in Japan Aerospace Exploration Agency, and exchanges the boundary information with neighboring sub-domains.

2.2 Computational Grid

An H-type structured grid is used for each blade passage, shown in Figure 1. In the case of stage analysis, the grids for individual passages overlap by one-mesh in the axial direction and the grid lines correspond to each other in the spanwise direction to reduce the two-dimensional interpolation process to circumferential linear interpolation process.

2.3 Boundary Conditions

At the upstream boundary, the radial profiles of total temperature, total pressure and flow angles are fixed as inflow boundary conditions. Static pressure is fixed at the exit boundary. Non-slip and adiabatic wall boundary conditions are applied to blade surface and hub/casing walls.

3 Fan Configurations

The fan design parameters are summarized in Table 1. The computational domain, which is composed of 18 rotor blades and 45 stator vanes, is reduced to a 1/9 sector of the annulus with 2 rotor blades and 5 stator vanes. Figure 1 shows an example of the computational grid for the unsteady stage analysis, in which total number of grids is about 4 million.

Table 1. Fan design parameters

Number of rotor blades		18
Number of staor vanes		45
Hub to tip ratio		0.55
Rotor tip	80% speed	0.95
Mach number	100% speed	1.18

Five different stator configurations with three sets of stator geometries, which are shown in Figure 2, are utilized in this study. Three radial stator configurations with different axial distance between the rotor and the stator use the same stator geometry. The radial stator with the shortest axial distance (0.5 rotor axial chord) is the baseline stator (A01). And the moved downstream radial stator (A02) and (A03) have the axial distance of one rotor axial chord and 1.5 rotor axial chord, respectively. The swept stator (B01), in which the stator has 20 degrees of sweep, has the same axial distance as the baseline stator (A01) at the hub and almost the same axial distance as the radial stator (A02) at the tip. And in the swept and leaned stator (C01), a stator lean of 30 deg in the direction of rotor rotation is incorporated into the swept stator (B01) for the upper 70 percent of the span.

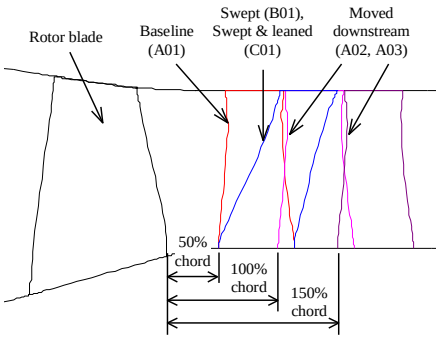

a. Meridional plane.

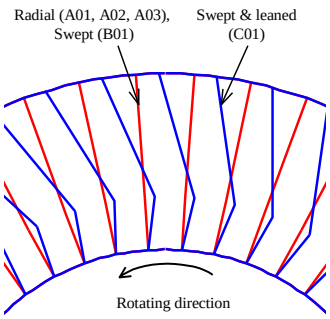

b. Axial plane (looking forward).

Figure 2. Schematic of the fan rotor and stator configurations.

4 Results and Discussions

4.1 Axial Spacing between Rotor and Stator

With increasing the axial spacing from A01 to A03, the rotor wakes at stator inlet decay. A Fourier analysis was carried out for the calculated rotor wakes at the stator inlet to obtain the disturbance velocity with a fundamental circumferential wave number. Figure 3 shows a comparison of the radially averaged magnitudes of the upwash component of the disturbance velocity between three radial stator configurations. In the figure, the comparison is made for 80 and 100 percent rotation speeds, in which the average magnitude is normalized by that of the baseline stator (A01) for each rotation speed. The calculation results show that the blade passing frequency (BPF) component of upwash velocity decreases in accordance with a power law, roughly in proportion to $L^{-4/5}$ at 80 percent rotation speed and L^{-1} at 100 percent rotation speed.

For a typical fan stage, a radial phase skew of the rotor wake usually occurs. Figure 4 shows rotor and radial stator on a blade-to-blade plane. A time required for the rotor wake to convect from the rotor trailing edge to the stator leading edge is given by L / V_x. Therefore the change in circumferential phase angle of the wake during the convection can be represented by

$$q = V_t \cdot \left(\frac{L}{V_x}\right) \cdot \left(\frac{1}{R}\right) \qquad (1)$$

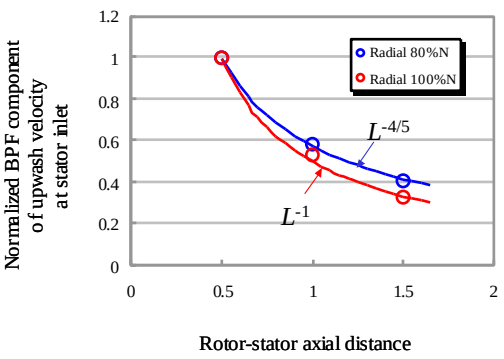

Figure 3. Comparison of radially averaged magnitudes of the upwash velocity at stator inlet.

If it is assumed that V_x at hub is equal to V_x at tip, then the difference in the circumferential phase angle between the hub and the tip can be expressed in the form

$$dq = q_{hub} - q_{tip} = \left\{\left(\frac{V_t}{R}\right)_{hub} - \left(\frac{V_t}{R}\right)_{tip}\right\}\frac{L}{V_x} \qquad (2)$$

From this equation, it is found that the variation in a radial phase skew of the rotor wake with the axial spacing is attributed to the difference in an angular velocity V_t / R between the hub and the tip and that the radial phase skew varies in proportion to the axial distance L. Figure 5 shows the rotor wake line at stator inlet obtained from the numerical calculations. It can be seen that the radial skew of the wake in the opposite direction of rotor rotation is increased as the axial spacing is increased. This is because the angular velocity of the swirl at hub $(V_t / R)_{hub}$ is larger than that at tip $(V_t / R)_{tip}$ for the fan model used in this study. The differences in the circumferential phase angle of a single rotor

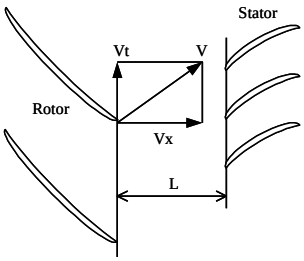

Figure 4. Schematic view of rotor and stator.

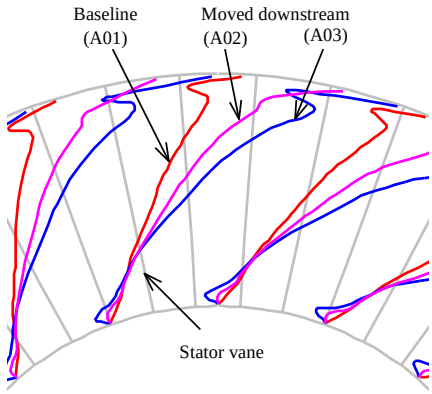

Figure 5. Rotor wakes at stator inlet at 100% rotation speed.

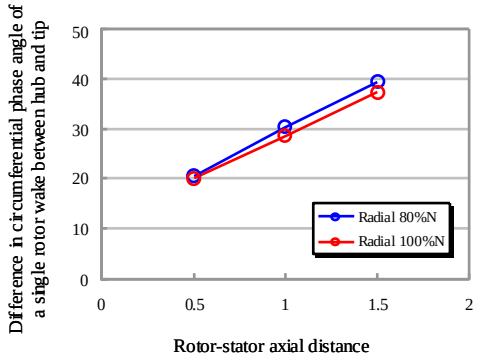

Figure 6. Differences in the circumferential phase angle of a single rotor wake between the tip and the hub.

wake between the tip and the hub are compared in Figure 6. The numerical calculation results show almost linear variation in the radial phase skew with increasing axial distance for both 80 and 100 percent rotation speed as indicated by equation (2). The results also show the same level of the radial skew between 80 and 100 percent rotation speed for each axial spacing. It is understandable from equation (2), because the numerical calculation results showed a similar swirl angle (that is V_x / V_t) at rotor exit between 80 and 100 percent rotation speed.

For the three radial stator configurations (A01, A02 and A03), the three-dimensional analytical prediction of unsteady pressures induced by the rotor wakes on the stator vanes was also conducted using an unsteady lifting-surface theory. The BPF component of the upwash velocity at 10 percent stator chord upstream from the stator leading edge was obtained from the numerical calculation results using a Fourier analysis, and used as an incoming sinusoidal gust in the analytical prediction. The radial phase skew of the rotor wake as shown in Figure 5 was also given in the analysis.

Figure 7 and 8 show surface contours of a BPF component of the unsteady pressure difference across the stator vane for the radial stator (A02) at 80 and 100 percent rotation speed, respectively. In each figure, a comparison between the analytical calculation and the numerical calculation is made. Left figure shows the amplitude of unsteady pressure difference across the stator vane, and center and right figures, respectively, are real and imaginary part of instantaneous unsteady pressure difference. Both numerical and analytical calculation results similarly show the distinctive features of the unsteady pressure distribution that, in addition to the leading edge region, some rounded regions of high amplitude pressure difference (red regions in the figure)

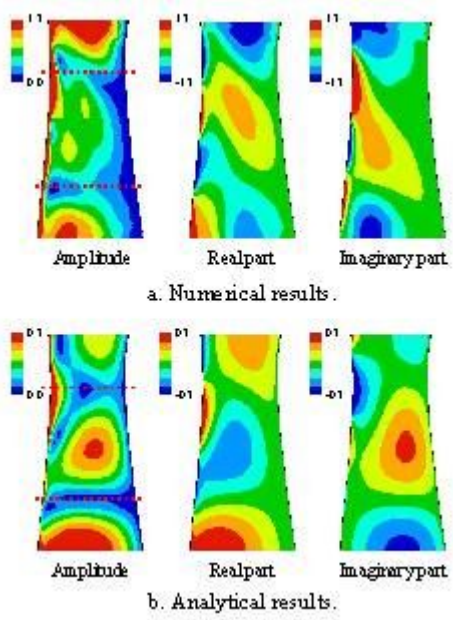

Figure 7. Surface contours of a BPF component of the unsteady pressure difference across the radial stator vane at 80% rotation speed.

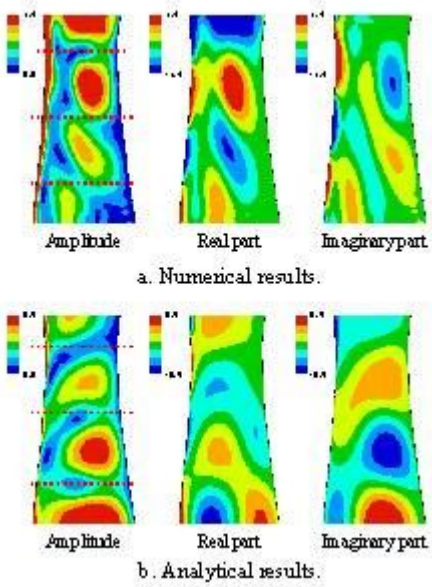

Figure 8. Surface contours of a BPF component of the unsteady pressure difference across the radial stator vane at 100% rotation speed.

appear in the spanwise direction near the mid-chord on a stator vane and that the number of high amplitude regions varies from three to four with changing the rotor rotation speed from 80 to 100 percent. Tsuchiya et al. suggested in Ref. [5] that this was attributed to three-dimensional effects, which could not be predicted by a two-dimensional approach. The nature of the distinctive distribution was also discussed by Tsuchiya et al. in Ref. [6].

In Figure 9, overall amplitudes of the BPF component of unsteady pressure difference across the stator vane, which were obtained by area-averaging of the local BPF amplitude over the stator surface, are compared between three radial stator configurations for both 80 and 100 percent rotation speed. The average amplitude is again normalized by that of the baseline stator (A01) for each rotation speed. In a quantitative comparison, the overall amplitudes obtained from the numerical calculation were considerably larger than those from the analytical calculation, however a comparison of the rate of decrease in the overall amplitude with increasing axial distance from the baseline stator shows a good agreement between the numerical calculation and the analytical calculation for both 80 (Figure 9a) and 100 percent rotation speed (Figure 9b). In the figure, the variation of incoming upwash velocity (Figure 3) is also plotted for each rotation speed. It can be seen that the rate of decrease in the unsteady pressure with increasing axial distance is larger than the rate of decay in the incoming upwash velocity for 80 percent rotation speed, whereas it is smaller for 100 percent rotation speed. In the lifting surface theory used in the analytical calculation, the effect of the magnitude of upwash velocity on the amplitude of unsteady pressure difference is linear. As seen in Figure 3, there is not a significant difference in the rate of decrease in the upwash velocity between 80 and 100 percent rotation speed. Therefore a remarkable difference in the rate of unsteady pressure reduction between these two rotation speeds may be attributed to the effect of radial phase skew of the rotor wake.

In order to clarify the effect of the phase skew of incoming rotor wake on the unsteady pressure difference, further calculations using the analytical method, in which only a phase skew of incoming rotor wake is varied with keeping upwash velocity component constant, were conducted for both 80 and 100 percent rotation speeds. Figure 10 shows the variation of resulting overall amplitude of unsteady pressure difference with the difference in the circumferential phase angle between the hub and the tip *dq*. In the figure, the overall

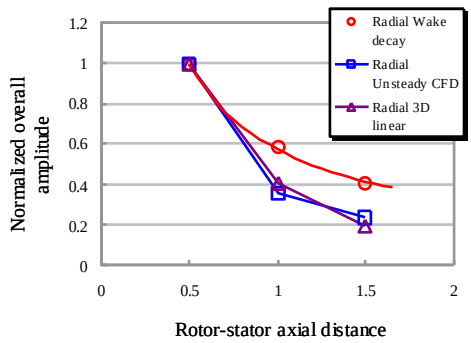

a. 80 percent rotation speed

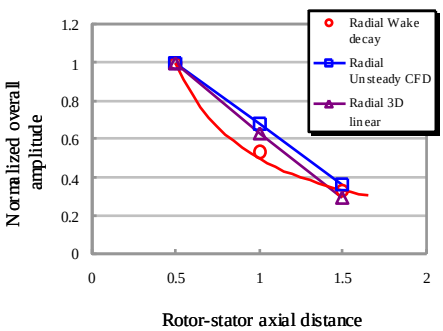

b. 100 percent rotation speed

Figure 9. Overall amplitudes of the BPF component of unsteady pressure difference across the stator vane.

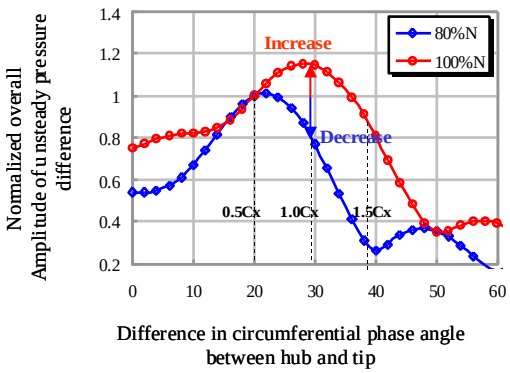

Figure 10. Variation of overall amplitudes of unsteady pressure difference with the difference in the circumferential phase angle between the hub and the tip *dq*.

amplitude is normalized by that at the *dq* of baseline stator (A01) in Figure 6 for each rotation speed (around 20 deg for both rotation speeds). It is found that the amplitude of unsteady pressure difference has a peak value at a certain *dq* and the *dq* at the peak differs depending on a rotation speed. The peak of 80 percent rotation speed locates near the *dq* of baseline stator (A01), so the unsteady pressure difference decreases at larger *dq*, that is, *dq* of radial stator (A02) and radial stator (A03). On the other hand, the peak of 100 percent rotation speed locates near the *dq* of radial stator (A02), therefore the unsteady pressure difference once increases from the *dq* of baseline stator (A01) to the *dq* of radial stator (A02) and then decreases. The consequent level of the unsteady pressure difference at the *dq* of radial stator (A03) is not much different from that at the *dq* of baseline stator (A01). These variations can clearly explain the reason why the reduction in unsteady pressure difference with increasing axial distance is significantly large compared with the decay in the incoming upwash velocity for 80 percent rotation speed, while the reduction is unexpectedly small for 100 percent rotation speed.

From the above investigations for the radial stator configurations with different rotor-stator spacing, it can be said that the effect of radial phase skew of incoming rotor wake should be carefully considered in determining an axial distance between rotor and stator.

4.2 Stator Sweep and Lean

The numerical predictions for the swept stator (B01) and the swept and leaned stator (C01) were also conducted for both 80 and 100 percent rotation speed. These two stators have the same sweep so that the stator leading edges are located at the same axial position along the span. The backward displacement of the leading edge from the baseline stator (A01) leading edge position allows the rotor wakes to decay further. Figure 11 shows the variation of radially averaged magnitudes of upwash velocity at 10 percent stator chord upstream

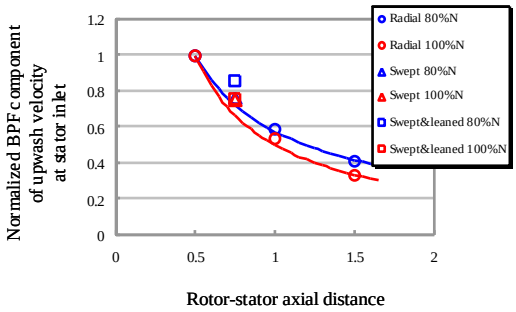

Figure 11. Comparison of radially averaged magnitudes of the upwash velocity at stator inlet.

from the stator leading edge with the rotor-stator axial distance. For both the swept stator and the swept and leaned stator, the upwash velocities are considerably decreased from the baseline stator (A01), but still larger than those for the radial stator (A02).

The radial phase skewing is also increased by a stator sweep as shown in Figure 13, but the reason is different from that in the case of a moved downstream radial stator. A schematic view of swept stator and the notation are shown in Figure 12. In the case of a backward swept stator, a time required for the rotor wake to

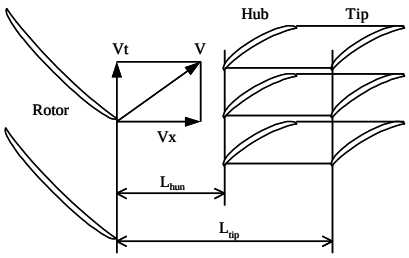

Figure 12. Schematic view of rotor and swept stator.

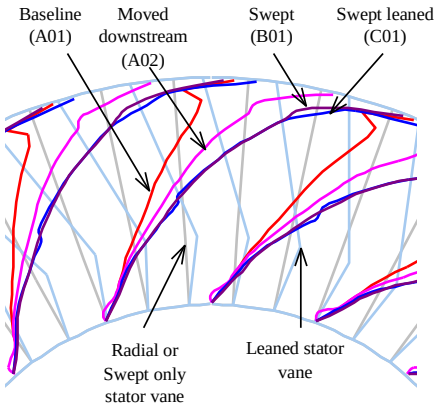

Figure 13. Rotor wakes at stator inlet at 100% rotation speed.

convect from the rotor trailing edge to the stator leading edge at tip is longer than that at hub. Therefore the tip portion of the rotor wake that has reached to the stator leading edge was discharged from the rotor trailing edge earlier than the hub portion that has reached to the stator leading edge at the same time. Then the change in circumferential phase angle of the wake at tip should be corrected as shown in equation (3).

$$q_{tip} = V_{t,tip} \cdot \left(\frac{L_{tip}}{V_x}\right) \cdot \left(\frac{1}{R}\right) - \Omega \cdot \left(\frac{L_{tip} - L_{hub}}{V_x}\right) \qquad (3)$$

Using the same assumption used in equation (2), the difference in the circumferential phase angle between the hub and the tip can be expressed in the form

$$dq = q_{hub} - q_{tip}$$
$$= \left\{\left(\frac{V_t}{R}\right)_{hub} - \left(\frac{V_t}{R}\right)_{tip}\right\}\frac{L_{hub}}{V_x} + \left\{\Omega - \left(\frac{V_t}{R}\right)_{tip}\right\}\frac{L_{tip} - L_{hub}}{V_x} \qquad (4)$$

$$\text{or } \left\{\left(\frac{V_t}{R}\right)_{hub} - \left(\frac{V_t}{R}\right)_{tip}\right\}\frac{L_{tip}}{V_x} + \left\{\Omega - \left(\frac{V_t}{R}\right)_{hub}\right\}\frac{L_{tip} - L_{hub}}{V_x} \qquad (5)$$

The first term of equation (4) is equivalent to the *dq* of the baseline stator (A01) and the second term is positive, because the angular velocity of rotor rotation is larger than the angular velocity of the swirl at tip. This

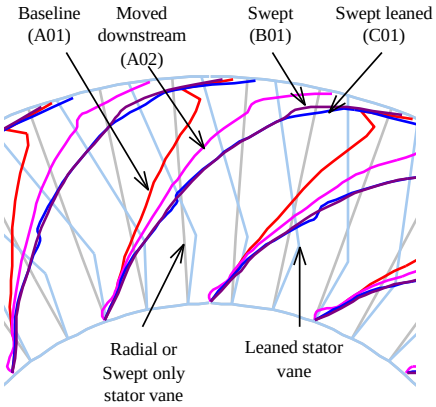

Figure 13. Rotor wakes at stator inlet at 100% rotation speed.

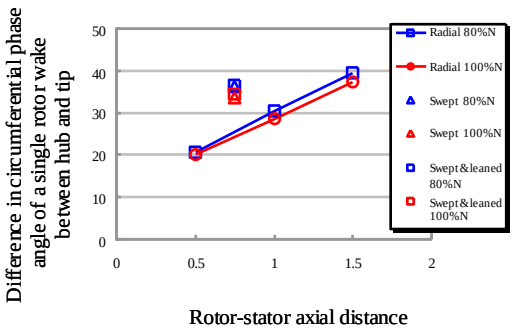

Figure 14. Differences in the circumferential phase angle of a single rotor wake between the tip and the hub.

indicates that the *dq* of swept stator is larger than the *dq* of baseline stator (A01). It is also indicated by equation (5) that the *dq* of swept stator is still larger than the *dq* of baseline stator (A02), because the positive second term, where the angular velocity of rotor rotation is still larger than the angular velocity of the swirl at hub in the current fan model, is added to the first term which is equivalent to the *dq* of the radial stator (A02). As seen in Figure 14, the resultant phase differences between the tip and the hub of swept stators obtained from the numerical calculations are larger than that for the baseline stator (A01), and still larger than that for the radial stator (A02) as indicated by equation (4) and (5).

Stator lean makes a difference in the number of individual rotor wakes that intersect a given stator vane. Figure 13 shows that the number of intersections is increased by one in the case of the swept and leaned stator compared with the swept stator.

In Figure 15, the surface contours of a BPF component of the unsteady pressure difference across the stator vane are compared between the baseline stator (A01) and the swept stator (B01) at 100 percent rotation speed. It can be seen that the amplitude of unsteady pressure difference near the leading edge is still high in the swept stator, however it is significantly decreased in the rounded regions of high amplitude pressure difference near the mid-chord. Figure 16 compares the surface contours of unsteady pressure difference between the swept stator (B01) and the swept and leaned stator (C01) at

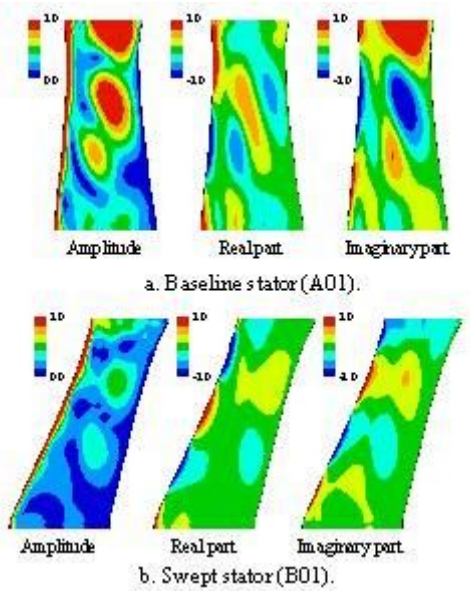

Figure 15. Comparison of surface contours of a BPF component of the unsteady pressure difference between the baseline stator (A01) and the swept stator (B01) at 100% rotation speed.

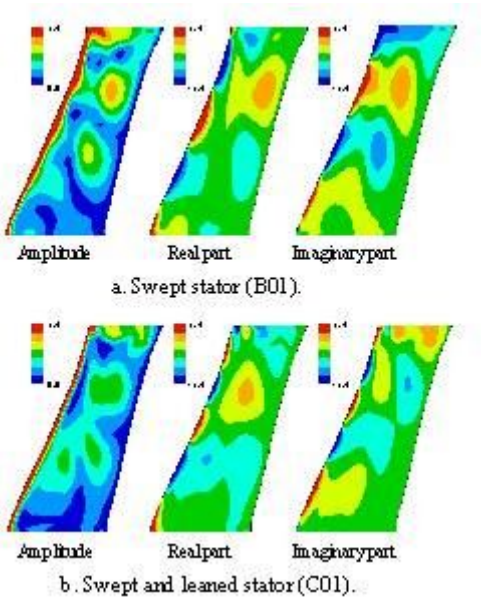

Figure 16. Comparison of surface contours of a BPF component of the unsteady pressure difference between the swept stator (B01) and the swept and leaned stator (C01) at 100% rotation speed.

100 percent rotation speed with different magnitude of the color from Figure 15. It can be also seen that incorporation of lean in the swept stator reduces the unsteady pressure difference mainly in the rounded regions near the mid-chord.

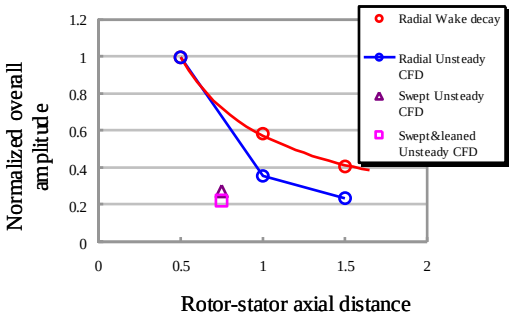

a. 80 percent rotation speed

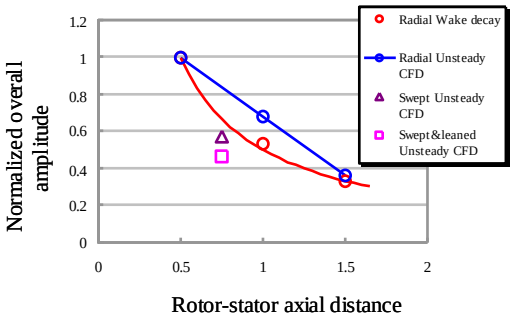

b. 100 percent rotation speed

Figure 17. Overall amplitudes of the BPF component of unsteady pressure difference across the stator vane.

In Figure 17, overall amplitudes of the BPF component of unsteady pressure difference across the stator vane for the swept stator and the swept and leaned stator are compared with the radial stator configurations for both 80 and 100 percent rotation speed. The average amplitude is again normalized by that of the baseline stator (A01) for each rotation speed. A significant decrease in the unsteady pressure difference from the baseline stator (A01) is shown for the swept stator (B01), but the rate of the decrease is different between 80 and 100 percent rotation speed. This may be due to the difference in variation of unsteady pressure difference with increasing *dq* between two rotation speeds, as observed in the radial stator configurations. As seen in Figure 11, the radially averaged magnitudes of upwash velocity for the swept stator (B01) are larger than those of the radial stator (A02) (about 30 and 40 percent larger, respectively, for 80 and 100 percent rotation speed) whereas the area-averaged amplitudes of unsteady pressure difference for the swept stator (B01) are about 20 percent smaller than those of the radial stator

(A02) for both 80 and 100 percent rotation speed. The difference in the *dq* between the swept stator (B01) and the radial stator (A02) seems to be too small (only about 5 deg for both 80 and 100 percent rotation speeds as seen in Figure 14) to explain that the difference in the amplitude of unsteady pressure between them. In a swept stator, there may be other beneficial effect for the unsteady pressure reduction than the effects of decay in rotor wake and increase in radial phase skew of rotor wake due to blade sweep.

It can be found from Figure 17 that the unsteady pressure reduction due to incorporation of lean in the swept stator is about 20 percent for both 80 and 100 percent rotation speed.

5 Conclusions

Unsteady three-dimensional Navier-Stokes analysis was conducted to predict the unsteady pressures induced by rotor viscous wakes on stator vanes. A three-dimensional analytical calculation using unsteady lifting-surface theory was also performed to elucidate the mechanism of the interaction.

1. In axial spacing between rotor and stator, the effect of radial phase skew of incoming rotor wake takes an important role in the reduction in the induced unsteady pressure. Increasing the radial phase skew doesn't always decrease the unsteady pressure.
2. Use of stator sweep and lean is an effective way to obtain a significant reduction in the induced unsteady pressure.
3. It is indicated that, in the use of a swept stator, there may be other beneficial effect for the unsteady pressure reduction than the effects of decay in rotor wake and increase in radial phase skew of rotor wake due to the blade sweep.

Acknowledgements

The authors would like to express their thanks to the New Energy and Industrial Technology Development Organization (NEDO) and the Ministry of Economy, Trade and Industry (METI), who gave them the opportunity to conduct "Research and Development of Environmentally Compatible Propulsion System for Next-Generation Supersonic Transport (ESPR) project".

References

[1] Woodward, R.P., et al., "Acoustic Benefits of Stator Sweep and Lean for a High Tip Speed Fan," AIAA-2002-1034, 2002.

[2] Envia, E., "Fan Noise Source Diagnostic Test - Vane Unsteady Pressure Results," AIAA-2002-2430, 2002.

[3] Namba, M., "Three-Dimensional Analysis of Blade Force and Sound Generation for an Annular Cascade in Distorted Flows," *Journal of Sound and Vibration*, No.50, No.4, pp.479-508, 1977.

[4] Kodama, H., and Namba, M., "Unsteady Lifting Surface Theory for a Rotating Cascade of Swept Blades," *Journal of Turbomachinery*, Vol.112, pp.411-417, 1990.

[5] Tsuchiya, N., Nakamura, Y., Yamagata, A., and Kodama, H., Nozaki, O., Nishizawa, T., and Yamamoto, K., "Fan Noise Prediction Using Unsteady CFD Analysis," AIAA-2002-2491, 2002.

[6] Tsuchiya, N., Nakamura, Y., Yamagata, A., and Kodama, H., Nozaki, O., Nishizawa, T., and Yamamoto, K., "Investigation of Acoustic Modes Generated by Rotor-Stator Interaction," AIAA-2003-3136, 2003.